



Short communication

Thermal expansion and steam oxidation of uranium mononitride analysed via in situ neutron diffraction



Jiatu Liu^a, Claudia Gasparrini^{a,b}, Joshua T. White^c, Kyle Johnson^d, Denise Adorno Lopes^d, Vanessa K. Peterson^{e,f}, Andrew Studer^e, Grant J. Griffiths^e, Gregory R. Lumpkin^e, Mark R. Wenman^b, Patrick A. Burr^a, Elizabeth S. Sooby^g, Edward G. Obbard^{a,*}

^a School of Mechanical and Manufacturing Engineering, UNSW, Sydney, NSW 2033, Australia

^b Department of Materials and Centre for Nuclear Engineering, Imperial College London, Exhibition Road, London SW 7 2AZ, United Kingdom

^c Material Science and Technology Division, Los Alamos National Laboratory, Los Alamos, NM, United States

^d KTH-Royal Institute of Technology, AlbaNova University Center, SE-106 91 Stockholm, Sweden

^e Australian Nuclear Science and Technology Organisation, Locked Bag 2001, Kirrawee DC, NSW 2232, Australia

^f School of Mechanical, Materials, and Mechatronic Engineering, University of Wollongong, Wollongong, NSW 2522, Australia

^g Department of Physics and Astronomy, University of Texas at San Antonio, San Antonio, TX 78249, United States

ARTICLE INFO

Article history:

Received 24 October 2022

Revised 19 December 2022

Accepted 20 December 2022

Available online 21 December 2022

ABSTRACT

In situ neutron powder diffraction experiments are applied to physical, kinetic, and microstructural characterization of uranium mononitride as a promising light water reactor fuel material. The temperature-variable coefficient of thermal expansion and isotropic Debye Waller factors are obtained by sequential Rietveld refinement over 499–1873 K. Oxidation of a UN pellet (95.2% density) under flow of 11 mg/min D₂O is observed to initiate above 623 K and the rate increases by a factor of approximately 10 from 673 to 773 K, with activation energy 50.6 ± 1.3 kJ/mol; uranium oxide is the only solid corrosion product.

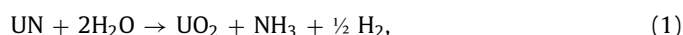
Crown Copyright © 2022 Published by Elsevier B.V. All rights reserved.

Uranium nitride is considered to be a long-term accident tolerant fuel technology,¹ due to the high uranium atom density (13.5 g-U/cc), high thermal conductivity that increases with temperature up to 1920 K [1], and high melting point at 1 atm N₂ (3035 K) [2]. The high uranium density of this fuel promotes longer cycle lengths at the current uranium enrichment while potentially enabling the use of a more corrosion resistant cladding. During normal operation, the enhanced thermal transport properties of UN lead to a reduced thermal gradient across the pellet for light water reactors (LWRs). Conventional UO₂ fuel has a uranium density of 9.67 g-U/cc and a thermal conductivity that decreases with temperature up to 2000 K [3].

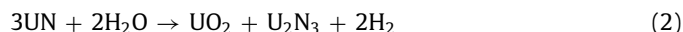
There is growing industrial interest in the development of UN for use in water cooled reactor fuel, and as such, it is crucial to understand the physical and chemical behaviour of UN as a fuel for building operational models, testing, and licensing for reactor use. The physical properties of UN have been summarised in a series of work by Hayes et al. [2,4–6], including lattice parameter, density, and mean linear thermal expansion coefficient obtained from variable temperature X-ray diffraction data. However, the limited

number of data points in these studies result in relatively high uncertainty for the reported coefficient of thermal expansion.

The challenges to the implementation of UN fuel include the requirement of enriching ¹⁵N (0.37% of natural abundant nitrogen) and, as a non-oxide in accident scenarios that involve a cladding breach [7], intrinsic instability in contact with the coolant. Hydrolysis of UN has been reported to occur as low as 473 K under uncontrolled steam flow [8]. The proposed reaction mechanism up to 873 K is:



With



as an intermediate reaction [8,9] The kinetics of the first reaction were studied under a steam flow of c.a. 0.1 mg/min (100 ml/min carrier gas and 30 torr steam partial pressure) at 613–693 K, revealing an activation energy of 88 kJ/mol [10]. More recent research on the corrosion of UN with a steam rate of 100 mg/min at 673–698 K demonstrated the effect of sample porosity on the reaction rate using in situ mass spectrometry of gaseous products (H₂, NH₃, N₂) [11], but did not quantify the reaction rate.

* Corresponding author.

E-mail address: e.obbard@unsw.edu.au (E.G. Obbard).

¹ <https://www.nrc.gov/reactors/atf/longer-term.html>.

In situ neutron diffraction is a powerful technique to characterize the transient behaviour of nuclear fuel compounds under imposed thermal or chemical conditions. Neutron scattering length and cross section are uncorrelated to atomic number, so unlike for X-ray diffraction the structure factor is sensitive to the composition and atomic coordinates in a unit cell even with high-Z, U atoms present. A thermal neutron beam easily traverses an aluminium alloy or steel sample environment apparatus, and a mini-fuel pellet sample of high-density U compound, to provide bulk composition, crystal structure, lattice parameter and quantitative phase analysis of the sample during an experiment. In comparison to thermogravimetric (TG) analysis [12], the results cannot be confounded by accumulation of water, or loss of material from the TG crucible. Phase fractions are obtained directly from Rietveld refinement, which involves fewer assumptions than inferring from mass gain. These advantages have seen neutron diffraction applied to the measurement and characterization of thermal expansion, atomic coordinates, and steam hydriding of U_3Si_2 [13–15].

In this study we apply in situ neutron diffraction to obtain 1) the coefficient of thermal expansion and 2) phase evolution kinetics of the reaction of UN with controlled steam flow.

In situ neutron diffraction experiments were performed on the high intensity neutron powder diffractometer Wombat [16] at the Australia Centre for Neutron Scattering (ACNS). A neutron beam of wavelength 1.6367(7) Å was employed in the thermal expansion experiment and 2.4136(9) Å in the steam corrosion experiment, as determined using the National Institute of Standards and Technology $La^{11}B_6$ 660b standard reference material [17].

The thermal expansion experiment used a uranium mononitride (UN) sample with a theoretical density of 96%, fabricated by spark plasma sintering (SPS) following the process outlined previously [18]. The UN powder was synthesized by hydriding-nitriding method which involves directly hydriding uranium metal followed by nitriding, both via gas-solid reaction. Impurities were analysed in the powder state by combustion using a LECO CS440 Determinator. Carbon was under 200 ppmwt and sulphur was below detection limits. Oxygen was measured by inert gas fusion using a LECO TC 436DR, at <500ppmw. Verification of elemental analysis after SPS does not reveal an appreciable change from the powder state for this fabrication route [18].

After grinding, the 5 mm high by 5 mm diameter cylindrical UN sample was inserted into an alumina container and loaded into a thin-walled vanadium cylinder and heated using an ILL-type high temperature vacuum furnace. The sample was heated to 1873 K at 4 K/min followed by cooling to 499 K at 4 K/min. Diffraction data were collected over 2 min periods continuously during the heating and cooling process.

The uranium mononitride sample for the steam corrosion experiment was prepared by sintering UN powder, by the method employed in [19]. The UN powder was prepared through carbothermic nitridation of uranium dioxide (UO_2). UO_2 powder was mixed with graphite powder and pressed using a 40 mm punch and die followed by high temperature treatment under vacuum to reduce UO_2 to UC. Subsequent heat treatments in N_2 and N_2/H_2 gas converted the UC to UN and consumed C impurities. UN powder was subsequently ball milled using Si_3N_4 milling media prior to 325 mesh sieving. Milled powders were pressed in a 5.84 mm punch and die set at 150 MPa and sintered in a W-mesh element furnace at 2473 K. Pellet density was found to be $94\% \pm 1\%$ using the ASTM B962 – 15 Archimedes principle. The carbon impurity, measured before sintering, was <1000 ppmwt and oxygen impurity after sintering 200 ppmwt [19].

For the corrosion experiment, the sample was placed in a customized stainless steel insert housed within an ILL-type high temperature vacuum furnace that allowed a flow of steam through the sample, with filtration systems for the retention of solids and gas

Table 1

Lattice parameter and U_{iso} obtained from Rietveld refinement for the two samples in this study.

	a_{UN} / Å	$100 \cdot U_{iso, N}$ / Å ²	$100 \cdot U_{iso, U}$ / Å ²
Thermal expansion	298 K 1873 K	4.8914(1) 4.9650(2)	0.3(2) 3.1(1)
Steam corrosion	298 K	4.897(8)	0.1(2) 1.9(1)

exhaust to radioactive waste. 11 mg/min D_2O flow was realized by flowing pure argon gas through a 333 K bath which was controlled by a Hidden Isochema XCS machine. The flow rate was kept constant throughout the experiment, i.e. during heating at 10 K/min to 623, 673, and 773 K with 6 h isothermal holds at each temperature. Diffraction data were collected over 1 min periods continuously during the experiment.

Neutron diffraction data were analysed using the General Structural Analysis System (GSAS) [20,21]. A pseudo-Voigt function including reflection asymmetry [22,23] was used to model peak shape in all data, where parameters contained combined instrumental and phase contributions. Important parameters that were refined include the GU , GV , GW for Gaussian broadening, LX , LY for Lorentzian broadening, as well as the $trms$ and $shft$ sample absorption and shift parameters, respectively.

Diffraction data from the thermal expansion experiment were analysed starting with the last dataset in the experiment, obtained after cooling (at 499 K). These patterns could be described using a multiphase structural model with UN ($Fm\bar{3}m$), Al_2O_3 ($R\bar{3}c$) and UO_2 ($Fm\bar{3}m$). The background was described by a six-term Chebyshev-type polynomial. Rietveld refinement was performed with peak profiles described by GU , GV , GW , LY and $shft$ for UN phase, GV , LX , LY , and $shft$ for Al_2O_3 phase, and $shft$ for the UO_2 phase. Lattice parameters and weight fractions were refined. Atomic coordinates and isotropic displacement parameters (U_{iso}) were refined for UN and Al_2O_3 phases. The remaining data from the thermal expansion experiment were analysed sequentially from this last pattern to the first (initial) dataset with all parameters fixed equal to those obtained from refinement of the final dataset, except for: phase weight fractions, the $shft$, U_{iso} , and lattice parameters for the UN and Al_2O_3 phases, and background terms.

Data from the corrosion experiment were also analysed sequentially starting with the last dataset. Data could be described using a multiphase structural model with structures for UN ($Fm\bar{3}m$) and UO_2 ($Fm\bar{3}m$) as described for the thermal expansion experiment. Peak profile parameters were obtained by analysis using the final data and fixed in the subsequent sequential refinement, except for the GP parameter for UN, the LY parameter for UO_2 , which were allowed to vary, and $shft$ for both phases, which were constrained equal. The lattice parameters and phase fractions were refined, as was the U_{iso} of U and N in the UN phase which was constrained to be equal.

Temperature-dependant in situ neutron diffraction data are shown as a contour plot in Fig. 1(a). Peak position changes arise from thermal expansion and peak intensity changes from the Debye-Waller effect [24,25]. All refinements had a goodness of fit χ^2 of 11.0 ± 1.2 . UO_2 of 0.9 ± 0.1 wt.% was found in the sample initially and increased to 1.6 ± 0.2 wt.% during the experiment, possibly from reaction with the alumina holder. The lattice parameter and U_{iso} parameters for the UN phase increase with temperature as shown in Table 1 and Fig. 1(b). U_{iso} measurement of U becomes meaningful when it exceeds its error value above 693 K. Pure UN lattice parameter at room temperature was reported previously as 4.8892 Å [26,27]. The difference of 2.2×10^{-3} Å between this and 4.8914 Å in Table 1 is significant in terms of Rietveld parameter uncertainty but could still be due to uncertainty in instrument configuration for pinpointing absolute lattice parameter. This has no effect on the measurement of thermal strains

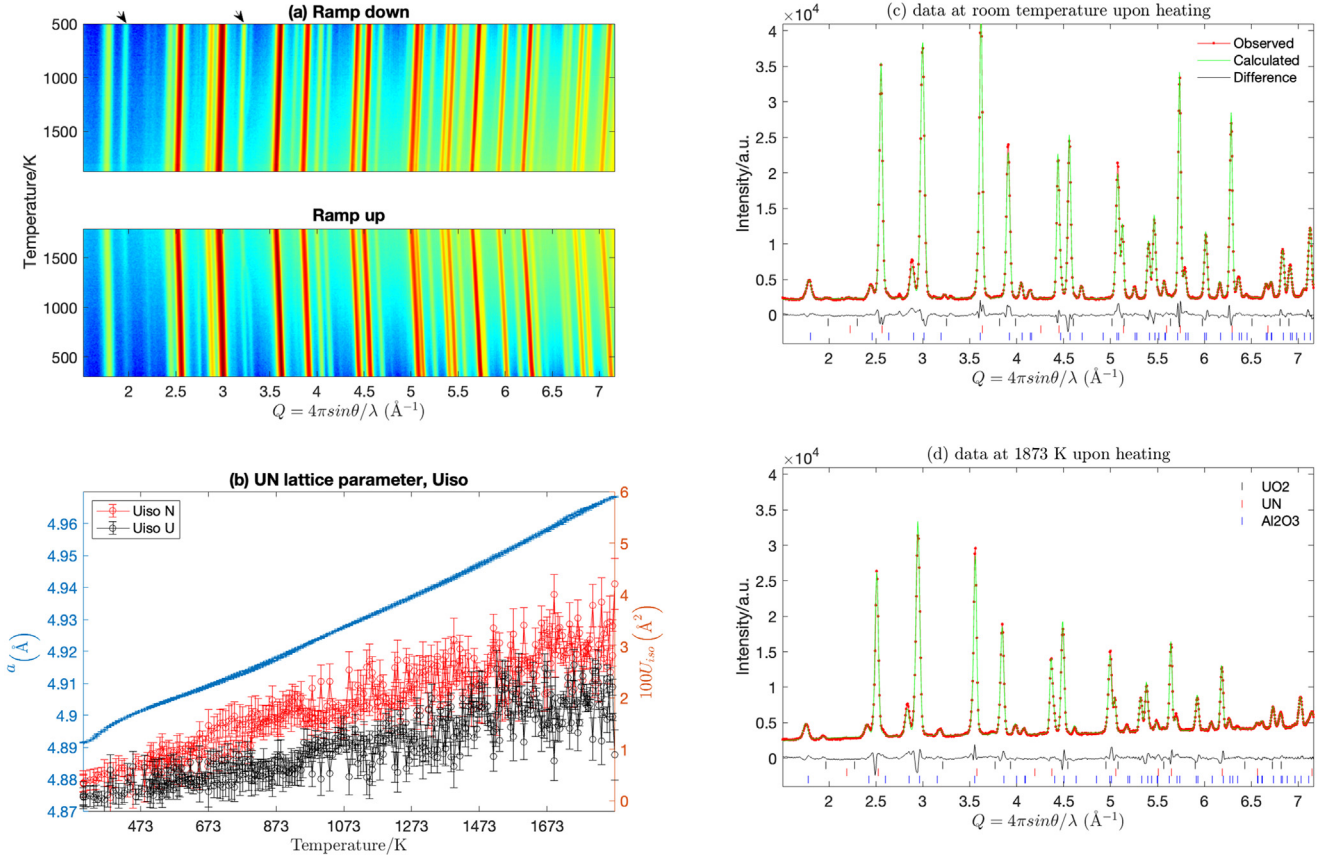


Fig. 1. (a) Contour plot of in situ diffraction data with intensity shown in colour from lowest (blue) to highest (red) displayed as log10 scale after a constant background is subtracted to enhance weak peaks; arrows identify reflections arising from the minor UO₂ phase; (b) UN lattice parameter and isotropic atomic displacement parameters U_{iso}; (c) (d) Rietveld refinement profiles using data at 298 and 1873 K; intensity is shown as arbitrary units (a. u.) and the legends inset apply to both plots.

with fixed instrument configuration. The measurement of impurity levels for the fabrication route described above and in [18] would suggest the discrepancy is not due to increase in UN lattice parameter caused by carbon, or oxygen [4,27]. Refinement profiles at low and high temperatures corresponding to Table 1 are shown in Fig. 1(c) and (d), respectively.

Coefficients of thermal expansion (CTE, α) were obtained by an expression describing the unit cell volume (V) over the temperature (T) [28]:

$$\alpha(T) = \frac{\partial \ln(V)}{\partial T} = \alpha_0 + \alpha_1 T + \alpha_2 / T^2 \quad (3)$$

With the integration form:

$$\ln\left(\frac{V_T}{V_{T_0}}\right) = \alpha_0(T - T_0) + \frac{1}{2}\alpha_1(T^2 - T_0^2) - \alpha_2(T^{-1} - T_0^{-1}) \quad (4)$$

The weighted least square fitting was carried out by taking into account errors associated with both $y = \ln(V_T/V_{T_0})$ and T , temperature readings [29]. Inverse variance σ_y^{-2} weighted least square fitting was conducted followed by iteration of $(\sigma_y + \alpha(T)\sigma_T)^{-2}$ weighted least square fitting until the differences of α_0 , α_1 , α_2 between consecutive steps of iterations are smaller than their errors. In our case, the convergence can be achieved in 2–4 iterations.

Fig. 2(a) and (b) presents the fitting results for UN using $T_0 = 499$ K with α_0 (linear model) and with α_0 and α_1 (quadratic model) for the heating and cooling ramps, respectively. Fitting a cubic model with α_0 , α_1 , and α_2 gave zero α_2 values within error, equivalent to the quadratic model. The quadratic model improves on the linear model in both cases in terms of χ^2 . The discrepancy between heating and cooling process may come from the vacuum

heating environment which produces non-stoichiometric uranium nitride within a narrow composition range [30]. Combining heating and cooling process data, we give our best quadratic fitting with $\chi^2 = 5.64$ for temperature range 499–1873 K:

$$\alpha(T) = \frac{\partial \ln(V)}{\partial T} = 1.97(1) \times 10^{-5} + 8.4(1) \times 10^{-9} \cdot T \quad (5)$$

To compare with the results by Hayes et al. ($a = 4.879 + 3.264 \times 10^{-5}T + 6.889 \times 10^{-9}T^2$ with the standard deviation of $\pm 0.026\%$ with respect to experimental data) [4,31,32], we fitted the lattice parameter correlation with temperature as shown in Fig. 2(c). Our linear model shows a standard deviation in lattice parameter of $\pm 0.023\%$ while the quadratic model that of 0.009%. The quadratic is:

$$a = 4.89(1) + 3.05(4) \times 10^{-5}T + 7.8(2) \times 10^{-9}T^2 \quad (6)$$

We now move to discussion of the steam corrosion experiment. A selection of in situ neutron diffraction data from the start of 623 K isotherm till the end of cooling are shown as a waterfall plot in Fig. 3(a) with the following data density: every 20 min during isothermal periods, every 10 min during cooling, and every 1 min during heating.

Typical Rietveld refinement profiles using data at room temperature and at the end of 773 K hold are presented in Fig. 3(b) and (c). Three UN reflections (indexed red in Fig. 3(a)) are identified as well as three broad reflections from UO₂ (indexed black in Fig. 3(a)). Table 1 includes the initial lattice parameter of this UN sample, which is within its error range of both the literature values and the first sample in this study. No U₂N₃ product as described by earlier research [8,10] is observed within our detection limit. This supports recent findings [33] of very little or no

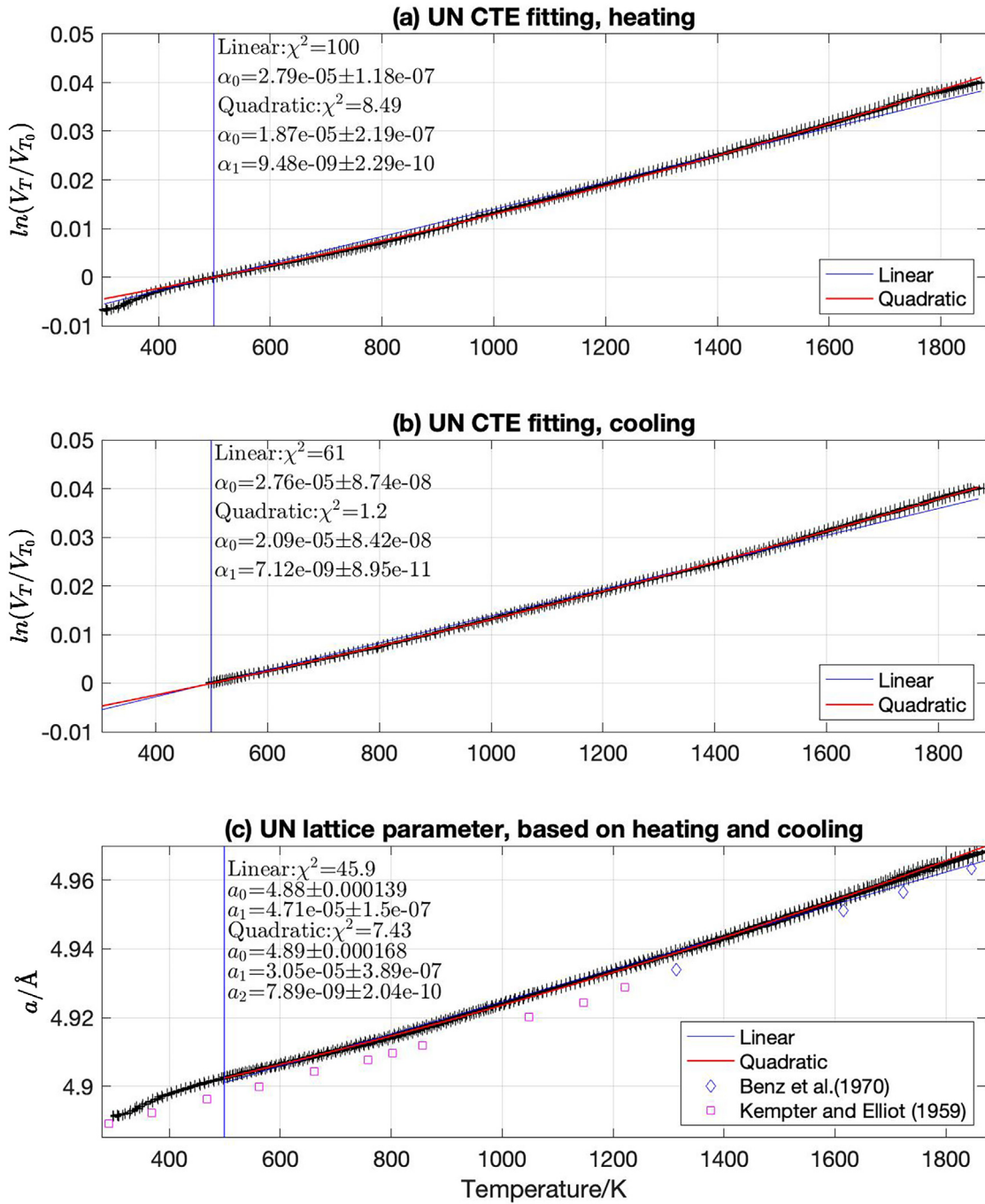


Fig. 2. Fitting coefficient of thermal expansion of UN as a linear equation $\ln(\frac{V_T}{V_{T_0}}) = \alpha_0(T - T_{T_0})$ and quadratic equation $\ln(\frac{V_T}{V_{T_0}}) = \alpha_0(T - T_{T_0}) + \frac{1}{2}\alpha_1(T^2 - T_{T_0}^2)$ above 499 K with $T_0 = 499$ K for data obtained during heating (a) and cooling (b); blue line indicates the lower temperature boundary for the fitting; (c) fitting lattice parameter of UN with temperature as a linear equation $a = a_0 + a_1T$ or as a quadratic equation $a = a_0 + a_1T + a_2T^2$ above 499 K with data during both heating and cooling. The blue line indicates the lower temperature boundary for the fitting; the insets show fitting parameters and $\chi^2 = \frac{1}{N_{obs} - N_{par}} \sum_i (y_i^{cal} - y_i^{obs})^2 / \sigma_{i,y}^2$; (c) includes data points from [31,32].

U_2N_3 present at any point during hydrothermal oxidation. Simulated neutron powder diffraction data based on our instrumental profile shows stronger peaks for U_2N_3 phase than for UO_2 phase, so it should be possible to identify, if present at a few tenths percent volume.

The intensity of UO_2 reflections increase due to reaction with steam following the 773 K hold. The wt.% of UN phase as a function of time is presented in Fig. 3(d). Three linear sections are observed, with the first revealing no statistically significant consumption of UN at 623 K. Increasing temperature from 673 to 773 K, UN

is consumed with the rate increasing by a factor of ten. These three rates of reaction (k_1 , k_2 , and k_3) are used to estimate an activation energy for the process (E_a) of 50.6 ± 1.3 kJ/mol based on an Arrhenius relation $k \sim e^{-E_a/RT}$ (where R is the universal gas constant). This value is lower than the 88 kJ/mol previously reported where UN powder was used with a much lower steam rate (0.1 mg/min) [10].

No peak shift besides thermal expansion, nor peak broadening, was observed during isothermal hold time, which excludes the possibility of steam hydriding as was observed for U_3Si_2 [15]. The

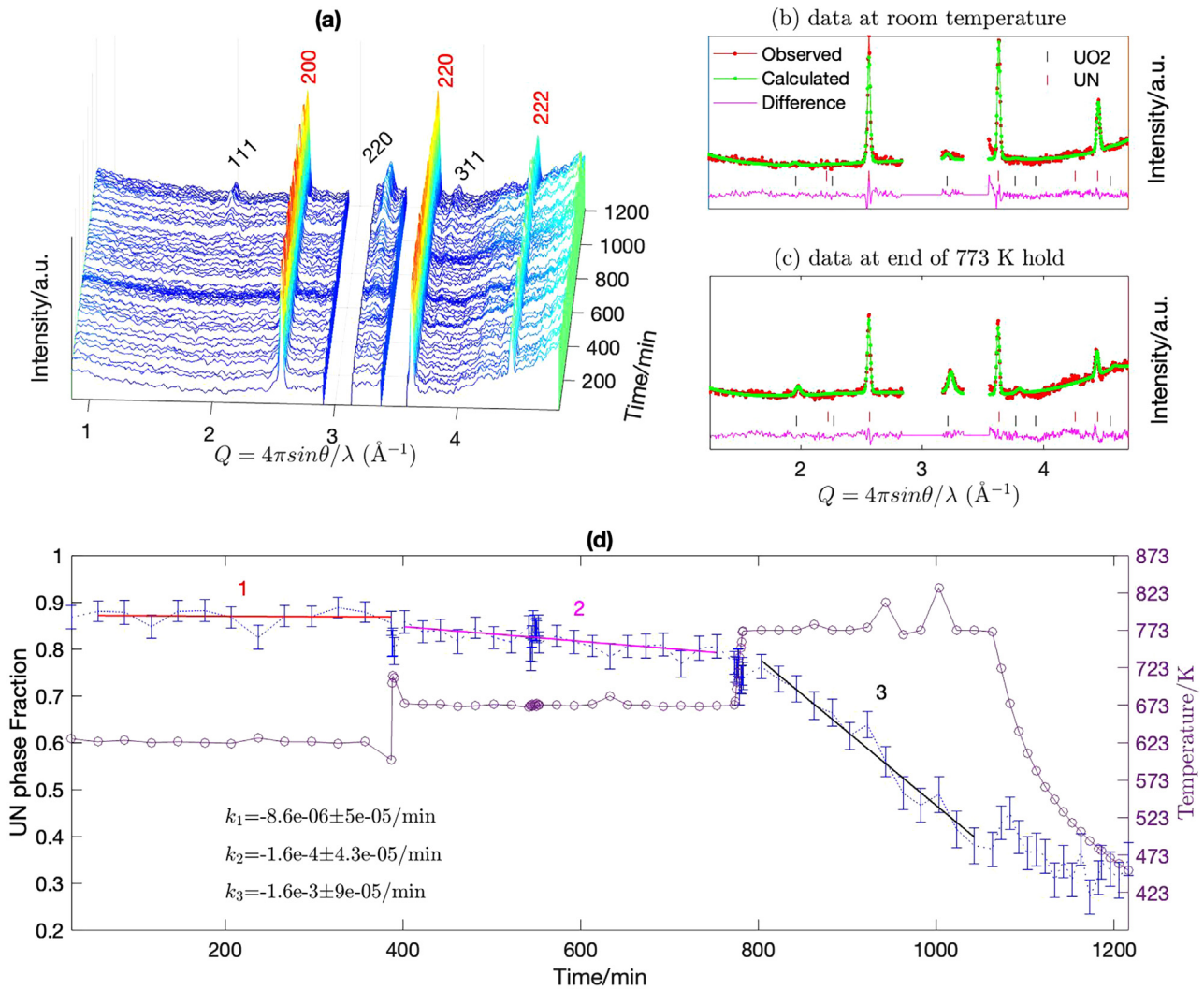


Fig. 3. (a) In situ neutron diffraction data from the UN corrosion experiment; intensity in colour from blue (lowest) to red (highest); (b) and (c) Rietveld refinement of neutron diffraction data of the UN sample at different stages of corrosion; the goodness of fit χ^2 is: (b) 2.350 and (c) 1.759; legend in (b) applies to (c) alike and peaks from steel container are omitted; (d) weight fraction of UN with temperature and time under constant steam delivery; three linear sections of the evolution of the UN phase fraction are identified as marked and fitted linearly with slopes k_1 , k_2 , and k_3 ; dashed lines through the temperature points are a guide to the eye.

UN material displays a linear, and kinetically retarded oxidation trend, in comparison to U_3Si_2 which shows rapid degradation at temperatures less than 673 K due to the combination of oxidation and hydride formation in water containing atmospheres [12,34].

The UN sample tested in this work displays a similar onset of degradation temperature in steam with those previously reported in [30,33]. Microstructural analysis of UN corroded in autoclave under steam at 573 K / 9 MPa [35] showed grain boundary corrosion with presence of UO_2 and a suggested mechanical disintegration of the pellet driven by increased volume of UO_2 compared to UN. Based on the current diffraction results, this is a 40% volume expansion when UN ($29.1 \text{ \AA}^3/U$) transforms to UO_2 ($40.875 \text{ \AA}^3/U$), hypothesized to disintegrate the pellet from grain boundary cracking.

The temperature range 623–773 K studied here coincides with the temperatures at the fuel-clad interface typical of a light water reactor, holding promise for UN as LWR nuclear fuel material, if protected from steam. In the event of steam ingress to pellets, oxidation proceeds from surfaces and near-surface grain boundaries, resulting in pellet fragmentation.

We demonstrated in this work how in situ neutron diffraction in a range of sample environments assists study of nuclear fuel materials with readily controlled radiation/contamination risks un-

der practical conditions: high temperature, and/or steam corrosive environment. By sequential Rietveld refinement on diffraction data of a UN pellet sample under vacuum heating and cooling, we derived the coefficient of thermal expansion (CTE) over the temperature range 499–1873 K in Eq. (5).

Compared with earlier CTE derived from diffraction method, we obtained much higher data density across the temperature range, giving more reliable fitting and precise characterization of instantaneous CTE.

From the diffraction data on a UN pellet sample under 11 mg/min steam flow and elevated temperatures, we found that the onset of corrosion is between 623 and 673 K. At 773 K the corrosion accelerates up to 10 times compared with that at 673 K. Unlike U_3Si_2 , no hydride was formed as the corrosion of UN is dictated by the diffusion of lattice oxygen instead of more mobile hydrogen. This means that UN could offer a promising high-U density fuel solution when the temperature at the fuel-cladding interface can be controlled under 623 K for normal operating temperatures, so that any steam ingress would not lead to chemical reaction.

Water/steam ingress at higher temperatures, will require further research to investigate the effects on nuclear fuel integrity. In situ neutron diffraction, embodied by two examples presented

here, is a promising technique for accelerating the development and licensing of nuclear fuels because it efficiently combines thermophysical, kinetic and microstructural characterization, under representative core conditions, with minimal handling of radioactive materials.

Author statement

Jiatu Liu: Formal analysis, Investigation, Writing - Original Draft. **Claudia Gasparri:** Formal analysis, Investigation, Writing - Original Draft. **Joshua T. White:** Conceptualization, Investigation. **Kyle Johnson:** Investigation, Writing - Review & Editing. **Denise Adorno Lopes:** Resources, Supervision. **Vanessa K. Peterson:** Methodology, Writing - Review & Editing. **Andrew Studer:** Methodology. **Grant J. Griffiths:** Methodology, Investigation. **Gregory R. Lumpkin:** Supervision, Project administration. **Mark R. Wenman:** Supervision, Funding acquisition. **Patrick A. Burr:** Supervision. **Elizabeth S. Sooby:** Conceptualization, Writing - Review & Editing. **Edward G. Obbard:** Conceptualization, Investigation, Writing - Review & Editing, Funding acquisition.

Declaration of Competing Interest

The authors declare that they have no known competing financial interests or personal relationships that could have appeared to influence the work reported in this paper.

The authors declare the following financial interests/personal relationships which may be considered as potential competing interests:

Data availability

Data will be made available on request.

Acknowledgements

The authors acknowledge contributions made by Chris Baldwin, Dr. Deborah Wakeham and Dr Daniel J. Gregg in the planning and execution of experiments; funding for beamtime proposals P6904 and P8186 at the Australian Centre for Neutron Scattering; CG and MRW: EPSRC funding under grant no. EP/P005101/1; CG: UNSW Sydney Women in Engineering Travel Award; EGO and PAB: funding from ANSTO and the Sir William Tyree Foundation.

References

- [1] S.B. Ross, M.S. El-Genk, R.B. Matthews, Thermal conductivity correlation for uranium nitride fuel between 10 and 1923 K, *J. Nucl. Mater.* 151 (1988) 318–326, doi:10.1016/0022-3115(88)90026-8.
- [2] S.L. Hayes, J.K. Thomas, K.L. Peddicord, Material property correlations for uranium mononitride: IV. Thermodynamic properties, *J. Nucl. Mater.* 171 (1990) 300–318, doi:10.1016/0022-3115(90)90377-Y.
- [3] C. Ronchi, M. Sheindlin, M. Musella, G.J. Hyland, Thermal conductivity of uranium dioxide up to 2900 K from simultaneous measurement of the heat capacity and thermal diffusivity, *J. Appl. Phys.* 85 (1999) 776–789, doi:10.1063/1.369159.
- [4] S.L. Hayes, J.K. Thomas, K.L. Peddicord, Material property correlations for uranium mononitride: I. Physical properties, *J. Nucl. Mater.* 171 (1990) 262–270, doi:10.1016/0022-3115(90)90374-V.
- [5] S.L. Hayes, J.K. Thomas, K.L. Peddicord, Material property correlations for uranium mononitride: II. Mechanical properties, *J. Nucl. Mater.* 171 (1990) 271–288, doi:10.1016/0022-3115(90)90375-W.
- [6] S.L. Hayes, J.K. Thomas, K.L. Peddicord, Material property correlations for uranium mononitride: III. Transport properties, *J. Nucl. Mater.* 171 (1990) 289–299, doi:10.1016/0022-3115(90)90376-X.
- [7] S.J. Zinkle, K.A. Terrani, J.C. Gehin, L.J. Ott, L.L. Snead, Accident tolerant fuels for LWRs: a perspective, *J. Nucl. Mater.* 448 (2014) 374–379, doi:10.1016/j.jnucmat.2013.12.005.
- [8] S. Sugihara, S. Imoto, Hydrolysis of Uranium Nitrides, *J. Nucl. Sci. Technol.* 6 (1969) 237–242, doi:10.1080/18811248.1969.9732878.
- [9] G.A.R. Rao, S.K. Mukerjee, V.N. Vaidya, V. Venugopal, D.D. Sood, Oxidation and hydrolysis kinetic studies on UN, *J. Nucl. Mater.* 185 (1991) 231–241, doi:10.1016/0022-3115(91)90340-D.
- [10] R.M. Dell, V.J. Wheeler, N.J. Bridger, Hydrolysis of uranium mononitride, *Trans. Farad. Soc.* 63 (1967) 1286–1294, doi:10.1039/tf9676301286.
- [11] M. Jolkkonen, P. Malkki, K. Johnson, J. Wallenius, Uranium nitride fuels in superheated steam, *J. Nucl. Sci. Technol.* 54 (2017) 513–519, doi:10.1080/00223131.2017.1291372.
- [12] E.S. Wood, J.T. White, C.J. Grote, A.T. Nelson, U_3Si_2 behavior in H_2O : part I, flowing steam and the effect of hydrogen, *J. Nucl. Mater.* 501 (2018) 404–412, doi:10.1016/j.jnucmat.2018.01.002.
- [13] E.G. Obbard, K.D. Johnson, P.A. Burr, D.A. Lopes, D.J. Gregg, K.-D. Liss, G. Griffiths, N. Scales, S.C. Middleburgh, Anisotropy in the thermal expansion of uranium silicide measured by neutron diffraction, *J. Nucl. Mater.* 508 (2018) 516–520, doi:10.1016/j.jnucmat.2018.04.049.
- [14] T.L. Ulrich, S.C. Vogel, J.T. White, D.A. Andersson, E.S. Wood, T.M. Besmann, High temperature neutron diffraction investigation of U_3Si_2 , *Materialia* 9 (2020) 100580, doi:10.1016/j.mta.2019.100580.
- [15] J. Liu, P.A. Burr, J.T. White, V.K. Peterson, P. Dayal, C. Baldwin, D. Wakeham, D.J. Gregg, E.S. Sooby, E.G. Obbard, Structural and phase evolution in U_3Si_2 during steam corrosion, *Corros. Sci.* 204 (2022) 110373, doi:10.1016/j.corsci.2022.110373.
- [16] A.J. Studer, M.E. Hagen, T.J. Noakes, Wombat: the high-intensity powder diffractometer at the OPAL reactor, *Physica B Condens. Matter.* 385–386 (2006) 1013–1015, doi:10.1016/j.physb.2006.05.323.
- [17] D.R. Black, D. Windover, A. Henins, J. Filliben, J.P. Cline, Certification of Standard Reference Material 660B, *Powder Diffraction* 26 (2011) 155–158, doi:10.1154/1.3591064.
- [18] K.D. Johnson, D.A. Lopes, Grain growth in uranium nitride prepared by spark plasma sintering, *J. Nucl. Mater.* 503 (2018) 75–80, doi:10.1016/j.jnucmat.2018.02.041.
- [19] E.S. Sooby, B.A. Brigham, G. Robles, J.T. White, S.W. Paisner, E. Kardoulaki, B. Williams, Steam oxidation of uranium mononitride in pure and reducing steam atmospheres to 1200 °C, *J. Nucl. Mater.* 560 (2022) 153487, doi:10.1016/j.jnucmat.2021.153487.
- [20] A.C.A.V.D.R.B. Larson, General Structure Analysis System (GSAS), Los Alamos National Laboratory, 2004 <https://subversion.xray.aps.anl.gov/EXPGUI/gsas/all/GSAS%20Manual.pdf>.
- [21] S.C. Vogel, gsa language: a GSAS script language for automated Rietveld refinements of diffraction data, *J. Appl. Crystallogr.* 44 (2011) 873–877, doi:10.1107/S0021889811023181.
- [22] L.W. Finger, D.E. Cox, A.P. Jephcoat, Correction for powder diffraction peak asymmetry due to axial divergence, *J. Appl. Crystallogr.* 27 (1994) 892–900, doi:10.1107/S0021889894004218.
- [23] B. van Laar, W.B. Yelon, The peak in neutron powder diffraction, *J. Appl. Crystallogr.* 17 (1984) 47–54, doi:10.1107/S0021889884011006.
- [24] P. Debye, Interferenz von Röntgenstrahlen und Wärmebewegung, *Ann. Phys.* 348 (1913) 49–92, doi:10.1002/andp.19133480105.
- [25] I. Waller, Zur Frage der Einwirkung der Wärmebewegung auf die Interferenz von Röntgenstrahlen, *Zeitschrift Für Physik* 17 (1923) 398–408, doi:10.1007/BF01328696.
- [26] T. Murofura, H. Tagawa, Lattice parameter of uranium mononitride, *J. Nucl. Mater.* 79 (1979) 264–266, doi:10.1016/0022-3115(79)90457-4.
- [27] M. Bradley Sears, Reactions of uranium carbonitrides and uranium nitride with aqueous solutions of hydrochloric, sulfuric, and nitric acids, *J. Inorg. Nucl. Chem.* 32 (1970) 2971–2984, doi:10.1016/0022-1902(70)80363-3.
- [28] G. Fiquet, P. Richet, G. Montagnac, High-temperature thermal expansion of lime, periclase, corundum and spinel, *Phys. Chem. Miner.* 27 (1999) 103–111, doi:10.1007/s002690050246.
- [29] P. Gans, *Data Fitting in the Chemical Sciences: By the Method of Least Squares*, Wiley, 1992.
- [30] J.K. Watkins, A. Gonzales, A.R. Wagner, E.S. Sooby, B.J. Jaques, Challenges and opportunities to alloyed and composite fuel architectures to mitigate high uranium density fuel oxidation: uranium mononitride, *J. Nucl. Mater.* 553 (2021) 153048, doi:10.1016/j.jnucmat.2021.153048.
- [31] R. Benz, G. Balog, B.H. Baca, UN lattice parameter at high temperature, *High Temp. Sci.* 15 (1970).
- [32] C.P. Kempter, R.O. Elliott, Thermal Expansion of $\langle UN \rangle$, $\langle UO_2 \rangle$, $\langle UO_2 ThO_2 \rangle$, and $\langle ThO_2 \rangle$, *J. Chem. Phys.* 30 (1959) 1524–1526, doi:10.1063/1.1730230.
- [33] E.S. Sooby, B.A. Brigham, G. Robles, J.T. White, S.W. Paisner, E. Kardoulaki, B. Williams, Steam oxidation of uranium mononitride in pure and reducing steam atmospheres to 1200 °C, *J. Nucl. Mater.* 560 (2022) 153487, doi:10.1016/j.jnucmat.2021.153487.
- [34] S. Mašková, K. Miliyanchuk, L. Havela, Hydrogen absorption in U_3Si_2 and its impact on electronic properties, *J. Nucl. Mater.* 487 (2017) 418–423, doi:10.1016/j.jnucmat.2017.02.036.
- [35] D.A. Lopes, S. Uygur, K. Johnson, Degradation of UN and UN- U_3Si_2 pellets in steam environment, *J. Nucl. Sci. Technol.* 54 (2017) 405–413, doi:10.1080/00223131.2016.1274689.